SCIENCE CHINA
Technological Sciences

• Article •

doi: 10.1007/s11431-016-0310-8

Responses of zonal wind at ~40°N to stratospheric sudden warming events in the stratosphere, mesosphere and lower thermosphere

YANG JunFeng[1,2], XIAO CunYing[1*], HU Xiong[1] & XU QingChen[1]

[1]*National Space Science Center, Chinese Academy of Sciences, Beijing 100190, China;*
[2]*University of Chinese Academy of Sciences, Beijing 100049, China*

Received April 20, 2016; accepted September 18, 2016; published online November 23, 2016

Based on the data at ~40°N at different longitudes during different stratospheric sudden warming (SSW) events, the responses of zonal winds in the stratosphere, mesosphere and lower thermosphere to SSWs are studied in this paper. The variations of zonal wind over Langfang, China (39.4°N, 116.7°E) by MF radar and the modern era retrospective-analysis for research and applications (MERRA) wind data during 2010 and 2013 SSW and over Fort Collins, USA (41°N, 105°W) by lidar and MERRA wind data during 2009 SSW are compared. Results show that the zonal wind at ~40°N indeed respond to the SSWs while different specifics are found in different SSW events or at different locations. The zonal wind has significant anomalies during the SSWs. Over Langfang, before the onset of 2010 and 2013 SSW, the zonal wind reverses from eastward to westward below about 60–70 km and accelerates above this region, while westward wind prevails from 30 to 100 km after the onset of 2010 SSW, and westward wind prevails in 30–60 and 85–100 km and eastward wind prevails in 60–85 km after the onset of 2013 SSW. Over Fort Collins during 2009 SSW, eastward wind reverses to westward in 20–30 km before the onset while westward wind prevails in 20–30 and 60–97 km and eastward wind prevails in 30–60 and in 97–100 km after the onset. Moreover, simulations by the specified dynamics version of the whole atmosphere community climate model (SD-WACCM) are taken to explain different responding specifics of zonal wind to SSW events. It is found that the modulation of planetary wave (PW) plays the main role. Different phases of PWs would lead to the different zonal wind along with longitudes and the different amplitudes and phases in different SSW events can lead to the different zonal wind responses.

stratospheric sudden warming (SSW), MF radar, WACCM, planetary waves

Citation: Yang J F, Xiao C Y, Hu X, et al. Responses of zonal wind at ~40°N to stratospheric sudden warming events in the stratosphere, mesosphere and lower thermosphere. Sci China Tech Sci, doi: 10.1007/s11431-016-0310-8

1 Introduction

The stratospheric sudden warming (SSW) event, first observed in 1952, is a dominant dynamical phenomenon in the northern hemisphere winter, occurring about every other year [1,2]. SSW may have significant global impacts on the whole atmosphere from stratosphere to mesosphere, thermosphere and ionosphere, coupling distinctly between the different regions with the profound changes of temperature, wind and constituents [3–10]. The mechanism for SSW events, now widely accepted, is that the planetary waves generate in the troposphere, propagate upward and dissipate through wave-mean flow interaction, producing strong westward forcing in stratosphere that leads the deceleration or reversal of the eastward winter winds in the stratosphere [11]. The deceleration and reversal of stratospheric winds changes the gravity wave filtering properties, and allows more eastward propagating gravity waves from lower atmosphere into the mesosphere and lower thermosphere (MLT), where gravity waves can break and deposit their

*Corresponding author (email: xiaocy@nssc.ac.cn)

momentum, resulting in the acceleration of zonal winds, upward/equatorward circulation and adiabatic cooling [12–15].

Most observations and studies of the evolution of the SSW are characterized and understood at high latitudes [16–20]. They have demonstrated that the characteristic variations of winds and temperature are associated with the SSW events from observations and simulations. In recent years, many studies are interested in the significant atmosphere changes over tropical latitudes [21–24] and mid-latitudes [25–28] during SSW. Chandran and Collins [29] studied the middle and low latitude effects of SSW events on temperature and zonal-mean winds in the middle atmosphere using a composite of SSW events between 1988 and 2010 by WACCM simulations. They showed the results that there is variability in observed zonal-mean winds and temperature depending on the location within or outside the displaced or split polar vortex and propagation direction of the planetary waves. Moreover, besides these general results coming from the model simulations, lots of observations from individual mid-, low- and high-latitudes during SSWs are encouraged to in-depth study how much and how the SSW process influence the atmosphere.

Along the longitude circle of ~40°N**,** there are some case studies about the observed responses of zonal wind to the SSWs. Yuan et al. [27] have shown the wind response of mesopause region over Fort Collins, USA (41°N, 105°W) to the 2009 SSW. Chen et al. [26] have reported the variability of MLT winds and waves over Langfang, China (39.4°N, 116.7°E) during 2010 SSW by MF radar wind data. Xiao et al. [30] have shown the response of the mesosphere and lower thermosphere wind over Langfang to the 2013 SSW by meteor radar wind data. All these studies show that the zonal wind at ~40°N have anomalies during the SSWs. However, all these studies focused on just one site in single event, and they mainly care about the responses in the MLT.

This paper is to investigate how much and how these observed anomalies vary from case to case and from individual location to location at ~40°N and the emphasis is the zonal wind response in the whole atmosphere, including stratosphere, mesosphere and lower thermosphere. The revolutions of zonal wind from 20 to 100 km are presented by combing the MLT observations with the local winds below MLT over from the modern era retrospective-analysis for research and rpplications (MERRA) data rather than the zonal mean zonal wind used in these papers [26,27,30]. In this study, local zonal wind over Langfang, China (39.4°N, 116.7°E) by MF radar with MERRA wind data during 2010 and 2013 SSW and the result over Fort Collins, USA (41°N, 105°W) by lidar in Yuan et al. [27] with MERRA wind data during 2009 SSW are adopted. Furthermore, simulations by the specified dynamics of whole atmosphere community climate model (SD-WACCM) are applied to explain different responding specifics of zonal wind to SSWs.

2 Data and analysis methods

2.1 Langfang MF radar

The MF radar at Langfang, China (39.4°N, 116.7°E) uses the spaced antenna system and employs full correlation analysis technique to routinely measure the horizontal winds [31]. The radar provides zonal and meridional winds from 60 to 100 km height range with height intervals of 2 km and time intervals of 4 min since June 2009. Table 1 gives the operational parameters of the MF radar. The radar operates at a frequency of 1.99 MHz with 64 kW peak transmitting power. Since the average number of wind estimates is low at 60–68 km in the daytime and at 60–80 km in the nighttime, wind data used in this work cover the height range 80–100 km.

The MF radar data are from 1 January 2010 to 28 February 2010 for the 2010 SSW and from 1 December 2012 to 28 February 2013 for 2013 SSW. The hourly winds are calculated from observations, and then are used to calculate the daily mean wind. The second procedure should have a minimum of 18 h of data. During the periods, the time series of the data are continuous.

2.2 MERRA

The modern era retrospective-analysis for research and applications (MERRA) is a reanalysis output of the Goddard Earth Observing System (GEOS-5) and data assimilation system (DAS) with version 5.2, developed by NASA. The included measurements in systems have various data types from ground- and space- based instrumentation, such as (special sensor microwave imager) SSM/I radiances and atmospheric infrared sounder (AIRS) radiances. MERRA data are in 6-h time interval and have horizontal resolution of 1/2° latitude by 2/3° longitude with 72 vertical levels from surface to 0.01 hPa. The details about MERRA data can be found in ref. [32].

The zonal winds between 20 and 78 km are extracted from MERRA at Langfang (39.4°N, 116.7°E). We then calculated daily mean of the extracted zonal wind, which are then used to combine with meteor radar observations in order to give the whole view of stratosphere, mesosphere

Table 1 Operational parameters of Langfang MF radar

Parameter	Value
Frequency	1.99 MHz
Peak transmitting power	64 kW
Pulse repetition frequency	80 Hz (day) /40 Hz (night)
Coherent integration	32 (day) /16 (night)
Height range	60–100 km
Range resolution	2 km
Time resolution	4 min

and lower thermosphere at Langfang in 2010 and 2013 SSW. The daily mean wind in the region 20–78 km at Fort Collins (41°N, 105°W) in 2009 SSW is also derived from MERRA.

2.3 WACCM

WACCM is a comprehensive global climate general circulation model, developed by the national center for atmospheric research (NCAR). In recent years, WACCM is embedded into the framework of community earth system model (CESM). The model extends from the earth's surface through the lower thermosphere (4.5×10^{-6} hPa, ~145 km) and has several standard horizontal resolutions. Planetary waves and other large-scale waves are resolved in the model while other small scaled fluctuations such as the orographic and non-orographic gravity waves are parameterized [33–36]. WACCM has been used to investigate the mechanisms about the responses to the SSWs in many studies [27,29].

WACCM simulations are taken in this paper to help to study the responses at mid-latitude to the 2013 SSW event and the dynamics causing the responses. WACCM are run in specified dynamics mode (SD-WACCM) by the resolution in the horizontal of 1.9° latitude by 2.5° longitude, and a variable vertical resolution, with 88 vertical levels [37]. SD-WACCM incorporates reanalysis data from observations in the troposphere and stratosphere. This study uses the horizontal winds and temperatures from GEOS-5 [38] to nudge. It is applied at every model time step (i.e., every 30 min). The simulation adopts 10% GEOS-5 fields in the nudging from surface to 50 km (0.79 hPa) and then linearly reduction between 50 and 60 (0.19 hPa) km. Above 60 km, the model becomes free running. Therefore, GEOS-5 temperature, zonal and meridional winds, and surface pressure are used in the model running to constrain their meteorological fields by controlling the boundary layer exchanges, advective and convective transport.

3 Results

3.1 Comparing the variations of zonal wind in the stratosphere, mesosphere and lower thermosphere during SSWs

In order to study the variations of zonal wind from 20 to 100 km over Langfang (39.4°N, 116.7°E), daily mean zonal winds derived from MF radar observations (80–100 km) and MERRA data (20–78 km) are combined together.

The time-altitude evolution of the daily mean zonal wind over Langfang from 20 to 100 km during the 2013 SSW is presented in Figure 1(a). The black straight line indicated the onset (6 January) of 2013 SSW at 60°N, 10 hPa. In the early and middle December 2012, the typical winter wind can be seen: eastward wind prevails in the upper stratosphere and mesosphere, reaching values of ~80 m/s at ~50 km; above this region, the zonal wind decreases and remains weak, alternating directions of eastward or westward. After 27 December 2012, zonal wind below 60–70 km decelerate rapidly, and reverse to westward before the onset at high latitude, accompanied by a strengthening of eastward wind above 70 km, reaching a peak value ~80 m/s. After the onset, the eastward wind above 60–70 km decelerates, reversing to westward above 85 km and remaining eastward below 85 km. the wind below 70 km remains westward, except for weak eastward wind in 8 January. The anomalies last for several days, and then return to the pre-SSW condition.

Figure 1(b) gives the evolution of zonal mean zonal wind in the region between 20 to 78 km at 40°N from the MERRA. In the winter condition, eastward wind dominates the height range in the Figure 1(b). Toward the end of December 2012, the zonal mean zonal wind decreases rapidly, and reaches weakest around the onset, only reversing in some limited regions. After the SSW, the wind returns to the condition before SSW.

Comparing the wind at Langfang in Figure 1(a) and the zonal mean zonal wind in Figure 1(b), the obvious differences during the 2013 SSW can be extracted: the wind at Langfang reverses below 60–70 km before the onset and in the regions 40–60 and 85–100 km after the onset, but the zonal mean zonal wind only reverses in several bulks around the onset; the former also has larger amplitude of westward wind than the later.

Figure 2(a) shows the time-altitude evolution of the daily mean zonal wind over Langfang from 20 to 100 km during the 2010 SSW. The black straight line indicated the onset (21 January) of 2010 SSW at 60°N, 10 hPa. In the early half of January, westward wind dominates the height region 20–60 km at most of the time before the onset at high latitude, in a reversal of the climatological mean zonal wind. At the same time, the zonal wind above 60 km shows eastward. After the onset, the reversal to westward wind is observed in the stratosphere, mesosphere and lower thermosphere, which is different with that in 2013 SSW. Several days later, the wind returns to the climatological condition.

The evolution of zonal mean zonal wind in the region between 20 to 78 km at 40°N during 2010 SSW is also given in Figure 2(b). The feature for 2010 SSW in the Figure 2(b) is similar to that for 2013 SSW in the Figure 1(b), except that the reversal in the height region 30–60 km in 2010 SSW is absent in 2013 SSW.

From the observations and the reanalysis data, the zonal wind has significant responses to 2010 and 2013 SSW at Langfang. While zonal mean zonal wind in the region 20–78 km decelerates rapidly during the SSWs, the wind in the stratosphere, mesosphere and lower thermosphere at Langfang has different changes before and after the onset with the zonal mean zonal wind: before the onset, the wind

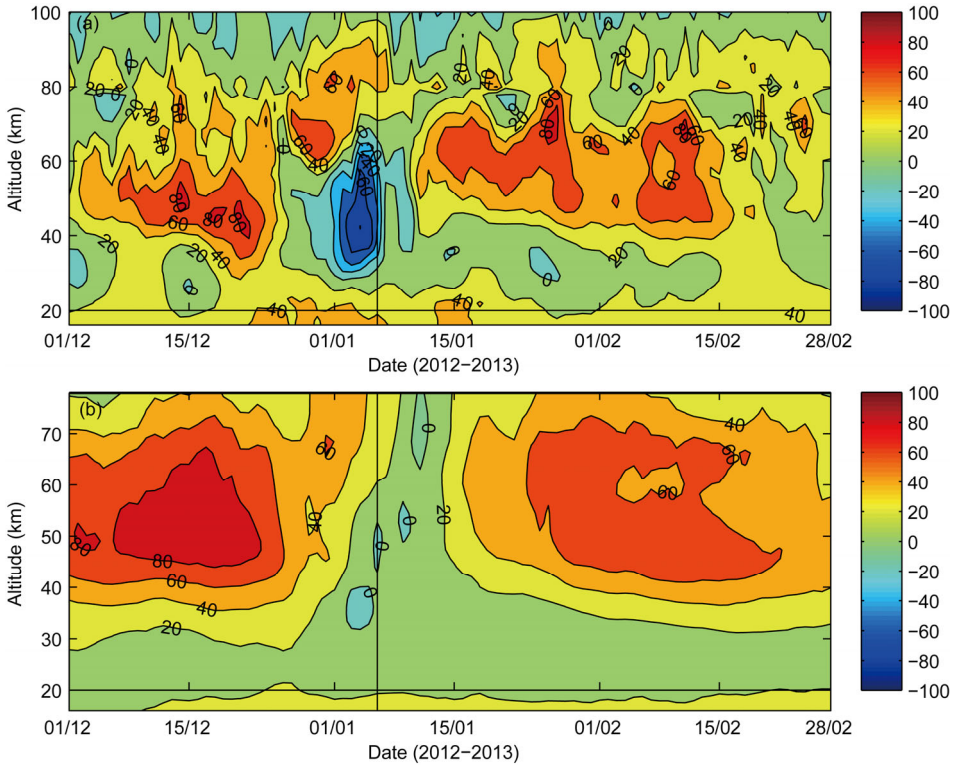

Figure 1 Time-altitude evolution of the daily mean zonal wind (m/s) at Langfang (39.4°N, 116.7°E) derived from MF radar observations (80–100 km) complemented with MERRA (20–78 km) (a) and zonal mean zonal wind (m/s) at 40°N in MERRA during 1 December 2012 to 28 February 2013 (b). The onset (6 January) at 60°N, 10 hPa and zero wind are indicated by a black straight line and black line, respectively.

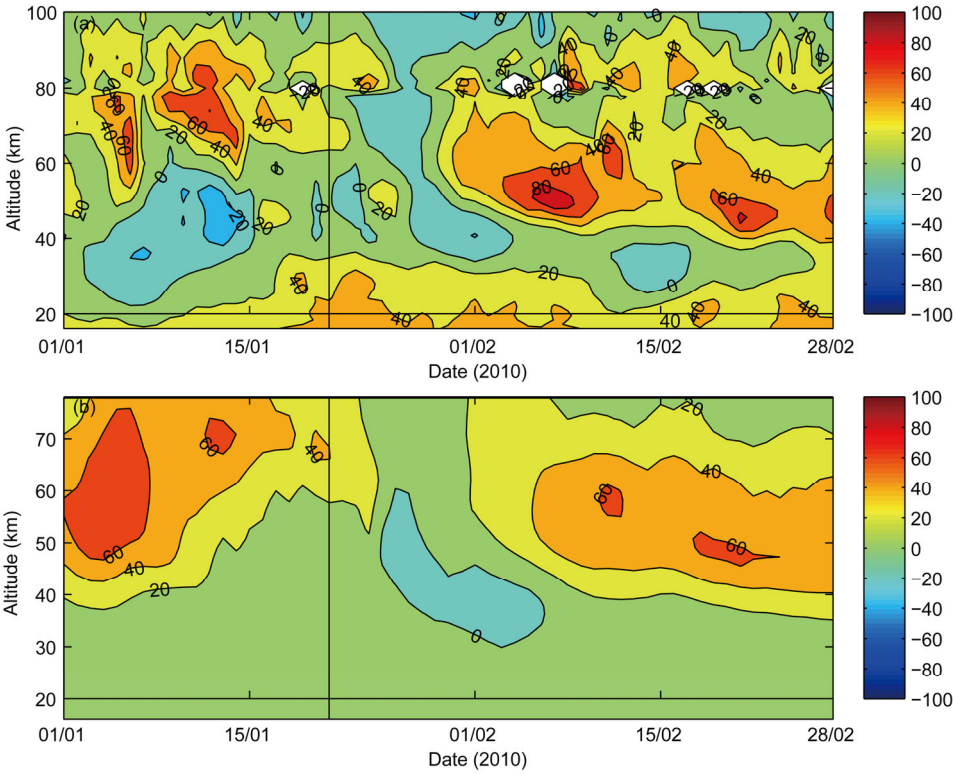

Figure 2 Time-altitude evolution of the daily mean zonal wind (m/s) at Langfang (39.4°N, 116.7°E) derived from MF radar observations (80–100 km) complemented with MERRA (20–78 km) (a) and zonal mean zonal wind (m/s) at 40°N in MERRA during 1 January 2010 to 28 February 2010 (b). The onset (21 January) at 60°N, 10 hPa and zero wind are indicated by a black straight line and black line, respectively.

below 60–70 km reverses from eastward to westward, and accelerates above the region; After the onset, the wind in the region 30–100 km reverses to westward in 2010 SSW for some days, whereas the westward wind region is separated by eastward wind at the altitude 60–85 km in 2013 SSW.

For the study about wind response to SSW at ~40°N, Yuan et al. [27] reported the wind reversed to westward from 80–97 km and turned to eastward above 97 km in a reversal of climatological mean wind profile from the observation of lidar at Fort Collins (41°N, 105°W) during the 2009 SSW. Fort Collins is about 138° of longitude away from Langfang and at similar latitude. Here, the evolutions of the local zonal wind at Fort Collins and zonal mean zonal wind in the region 20–78 km at 41°N are presented in Figure 3(a) and (b). The onset (21 January) of 2009 SSW at 60°N, 10 hPa is marked by a straight back line. In the Figure 2(b) in Yuan et al. [27], the variation of the mean wind during the period from 04:16 of 19 January and 07:48 of 21 January is shown. The mean zonal wind shows relatively weak westward winds in most of the mesopause region, and returns from westward to eastward near the end 19 January above 95 km. Uniting their observation with the Figure 3(a) in this paper, the brief zonal wind evolution can be documented: before the onset, the wind reverses only in the region below 30 km, without regard to the region above 78 km for the absent of observation; around the onset, the regions 20–30 and 60–95 km is dominated by westward wind, and the other regions by eastward wind. The zonal mean zonal wind acts the deceleration during the 2009 SSW as same as that during 2010 and 2013 SSW, but with lager reversal region.

In summary, the MF radar observation and MERRA reanalysis data show significant responses of zonal wind at Langfang and zonal mean zonal wind at mid-latitude, as well as the study by Yuan et al. [27]. While the zonal mean zonal wind acts with the similar feature, the anomalies during the SSWs are various, which are described above. It is known that the SSW is associated with planetary waves closely. Jacobi et al. [25] noted that the effect of the SSW may depend on the position of the vortex relative to the observational sites. So, we can use the SD-WACCM to simulate 2013 SSW to get the global perspective, and investigate the dynamical mechanisms. The effect on the responses of observational sites by planetary waves is discussed.

3.2 SD-WACCM simulation of 2013 SSW

Figure 4 shows the evolution of zonal wind in the region 20–100 km at Langfang and zonal mean zonal wind at 40ºN during 2013 SSW derived from SD-WACCM simulation. Since the MERRA is similar with the GEOS-5 used to nudging below 60 km in the SD-WACCM, the states below 60 km in the Figure 4 is in accordance with that in Figure 1.

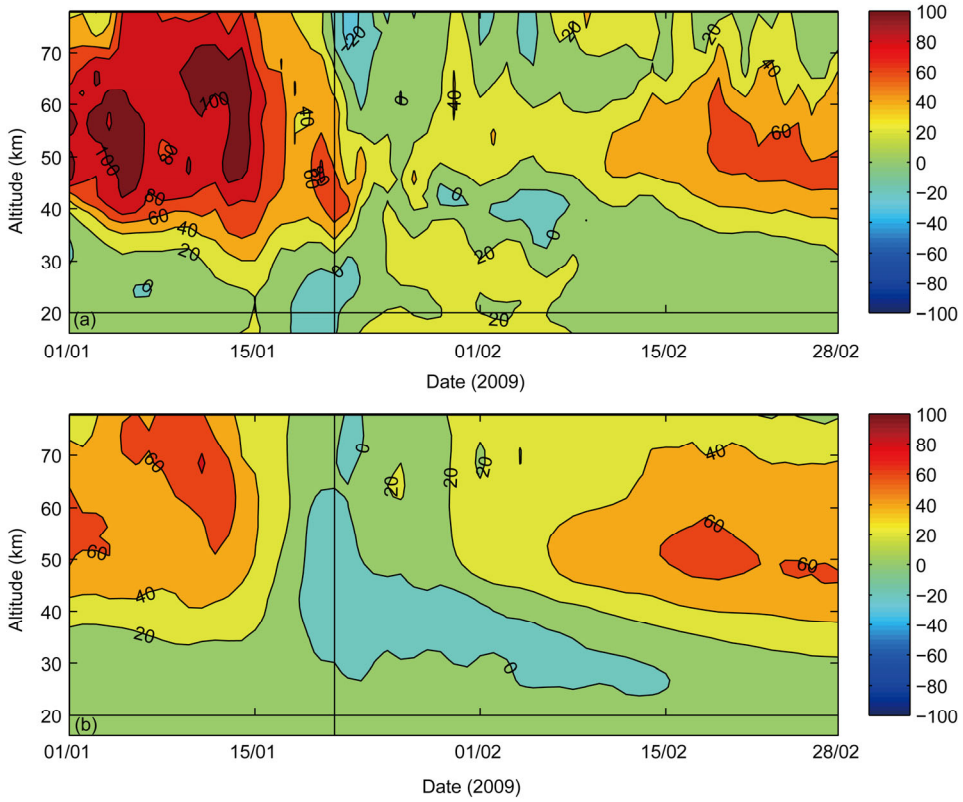

Figure 3 Time-altitude evolution of the daily mean zonal wind (m/s) at Fort Collins (41ºN, 105ºW) in MERRA (20–78 km) (a) and zonal mean zonal wind (m/s) at 40°N in MERRA during 1 January 2009 to 28 February 2009 (b). The onset (21 January) at 60°N, 10 hPa and zero wind are indicated by a black straight line and black line, respectively.

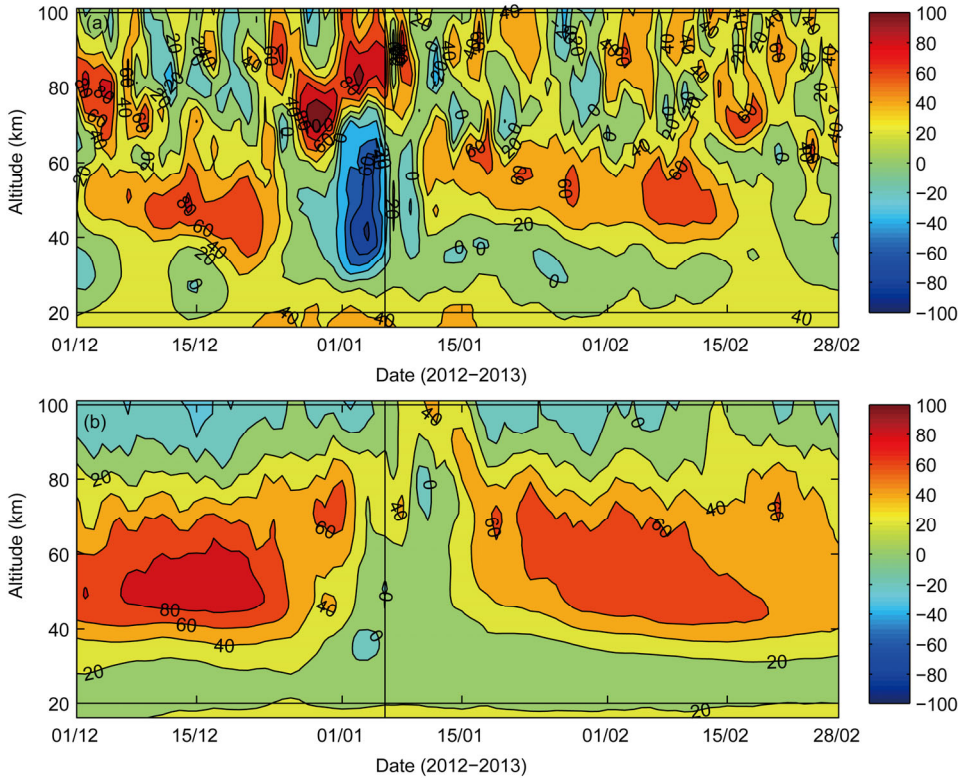

Figure 4 Time-altitude evolution of the daily mean zonal wind (m/s) at Langfang (39.4°N, 116.7°E) (a) and zonal mean zonal wind (m/s) at 40°N derived from SD-WACCM simulation during 1 December 2012 to 28 February 2013 (b). The onset (6 January) at 60°N, 10 hPa and zero wind are indicated by a black straight line and black line, respectively.

Above 60 km, the model also generally captures the characteristic wind evolution at Langfang that acceleration, only with some detailed differences, such as the larger eastward wind before the onset and the absence of reversal above 80 km after the onset.

The geopotential height amplitudes of planetary wave number 1 (PW1, Figure 5(a)) and wave number 2 (PW2, Figure 5(b)) at mid-latitude (40°N) during 2013 major SSW are also deduced from SD-WACCM simulation. The geopotential height amplitudes of PW1 are large in upper stratosphere and lower mesosphere but small in above regions in December 2012. The amplitudes of PW1 increase rapidly in the stratosphere, mesosphere and lower thermosphere before the onset, reaching max values of ~900 m, and decrease slowly after the onset. The geopotential height amplitudes of PW2 are small before the onset and increase rapidly at most regions after the onset, reaching peak value of ~900 m at 50 and 90 km.

The transform Eulerian mean diagnostic framework is used to examine the planetary wave forcing by calculating the divergences of the Eliassen-palm (EP) flux of PW1 and PW2 [39]. Figure 6 shows the forcing produced by the planetary on zonal mean zonal wind. In the clamatological winter condition in the early of December 2012, The PW1 and PW2 make relatively weak forcing with small variations (from –20 to 20 m/s/d). During the SSW, through wave-mean flow interaction, the PW1 produces a strong westward forcing with maximum of –60 m/s/d at ~70 km before the onset (Figure 6(a)), whereas the PW2 produces a westward forcing with peak values of –40 m/s/d at ~60 km and –60 m/s/d at ~90 km after the onset (Figure 6(b)). By the effects from westward forcing of PW1 and PW2 in succession, the zonal mean zonal wind in the height from 30 to 85 km decelerates or reverses in the Figure 4. The above wind change also allows more eastward propagating gravity waves into the MLT. The eastward momentum forcing produced by breaking of gravity waves (not shown) is larger than westward forcing by planetary waves in the lower thermosphere, leading an acceleration of zonal wind above 85 km in simulation (Figure 4(b)).

A comparison of the zonal mean zonal wind and the geopotential amplitudes of PW1 and PW2 at 40°N with corresponding results at 60°N is also made. At high latitude, the winter eastward wind decelerates with bigger amplitude than that at mid-latitude, showing a prolonged and widespread reversal. The difference of zonal mean zonal wind can be explained by the distribution of planetary waves. The amplitudes of PW1 and PW2 at 60°N can reach twice as big as that at 40°N, producing a much stronger westward forcing than the later.

Figure 7 displays the distributions of zonal wind in the simulation at 32 km (~10 hPa, left column), 60 km (~0.19

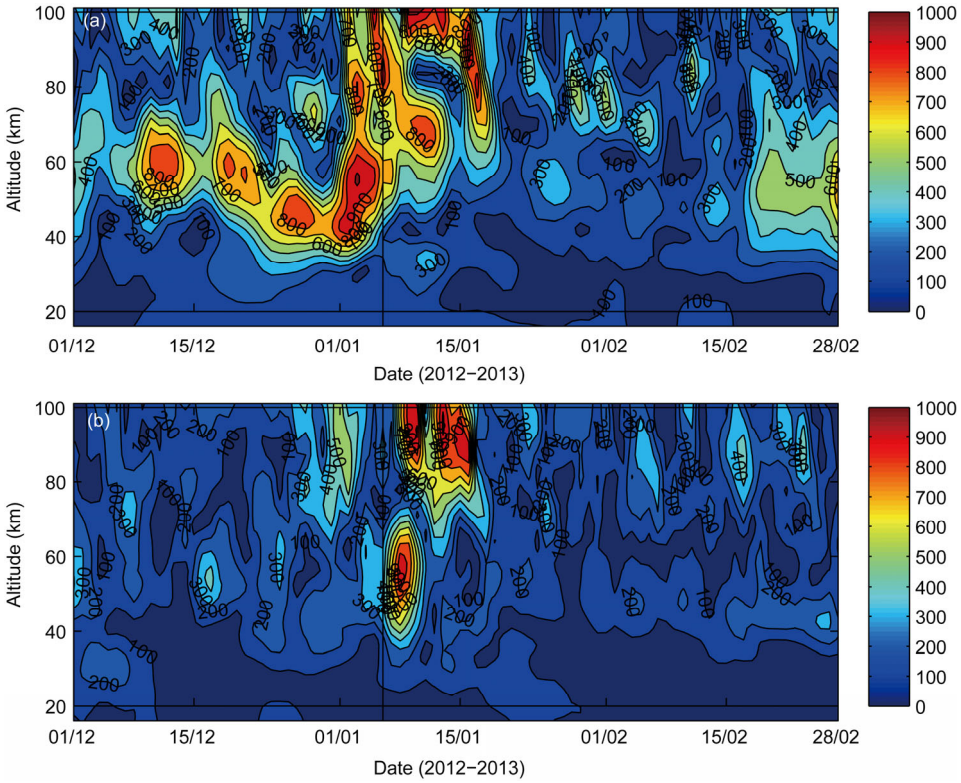

Figure 5 Time-altitude evolution of the geopotential height amplitudes (m) of planetary wave number 1 (PW1) (a) and wave number 2 (PW2) (b) at 40°N in SD-WACCM simulation from 1 December 2012 to 28 February 2013. The onset (6 January) at 60°N, 10hPa is indicated by a black straight line.

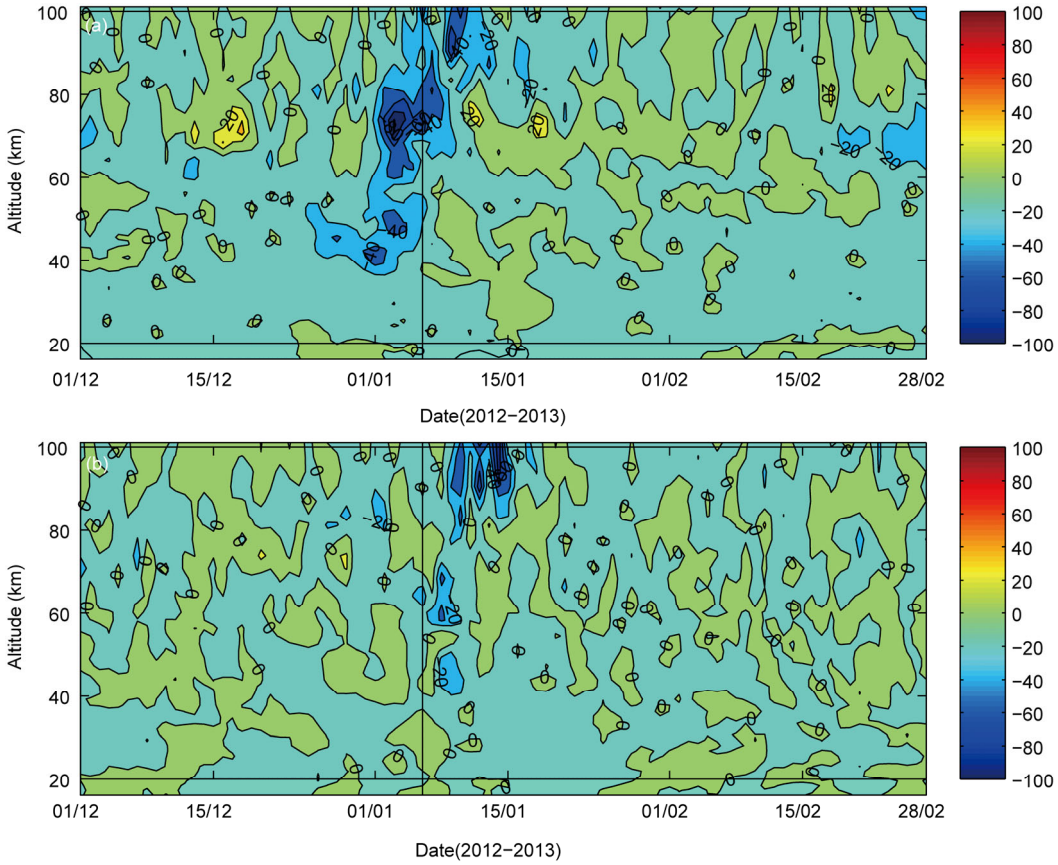

Figure 6 Time-altitude evolution of the forcing by the PW1 (a) and PW2 (b) at 40°N in SD-WACCM simulation from 1 December 2012 to 28 February 2013. The onset (6 January) at 60°N, 10 hPa and zero forcing are indicated by a black straight line and black line, respectively.

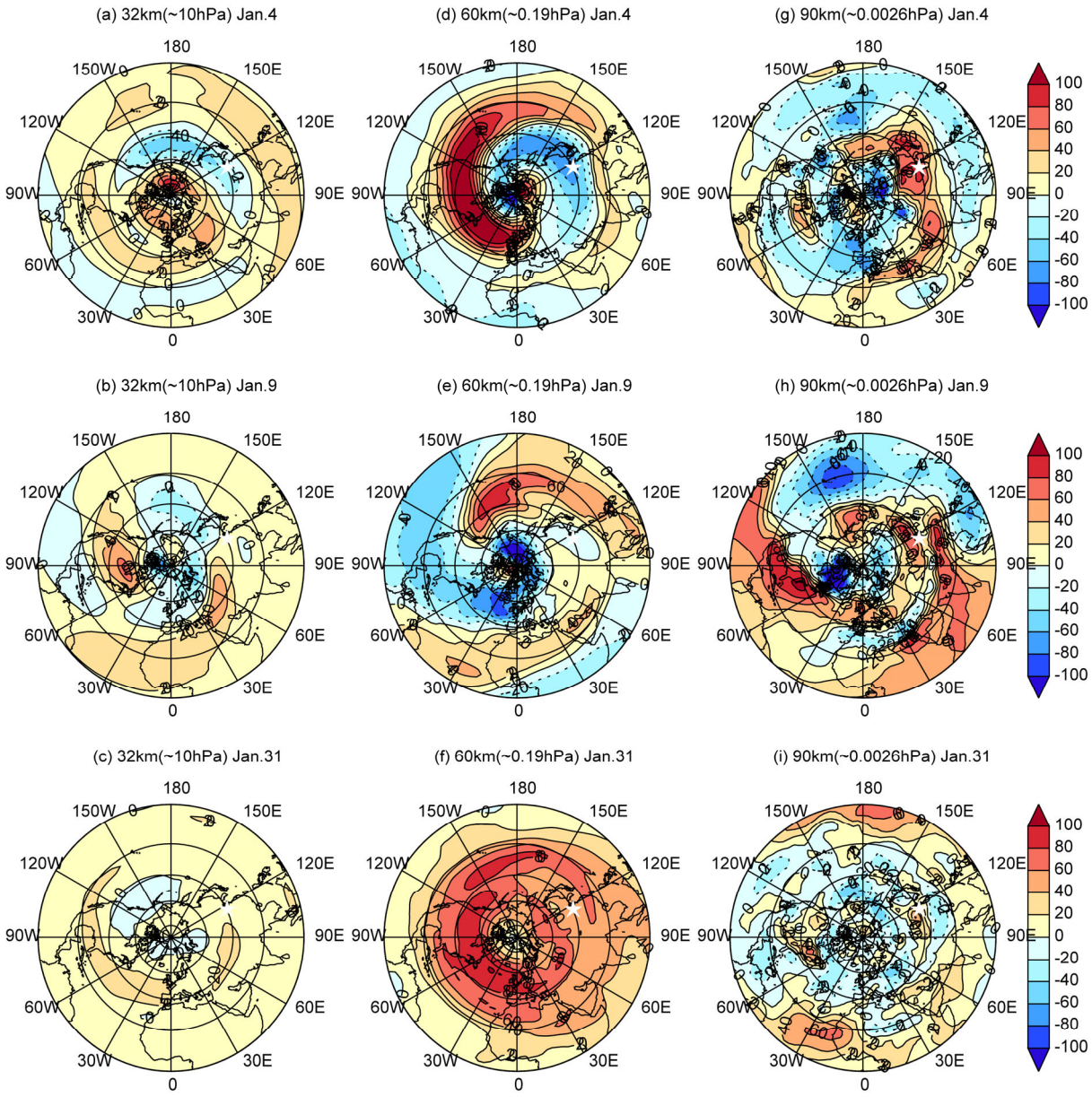

Figure 7 The distributions of zonal wind (m/s) in the SD-WACCM simulation at 32 km (~10 hPa) ((a)–(c)), 60 km (~0.19 hPa) ((d)–(f)) and 90 km (~0.0026 hPa) ((g)–(i)), for ((b),(d),(g)) 4, ((b),(c),(h)) 9 and ((c),(f),(i)) 31 January 2013. The location of Langfang (39.4°N, 116.7°E) is marked by white star.

hPa, middle column) and 90 km (~0.0026 hPa, right column), for 4, 9 and 31 January 2013 in top, middle and bottom rows. Three altitudes represent the stratosphere, mesosphere and lower thermosphere respectively. These figures are helpful to understand the relationship between the local zonal winds over Langfang (marked with white star in figures) and global wind structure in 2013 SSW. In the stratosphere, the polar vortex displaces before the onset and splits after the onset, which showing PW1 and PW2 structures respectively. The effects of planetary waves extend from the North Pole to ~20°N. In the mesosphere, there is also a vortex displacement and a vortex split. The PW1 and PW2 structures can be seen from the North Pole to tropical regions. In the lower thermosphere, an anticyclone dominates the North Pole in climatologically winter condition, and then displaces before the onset, and splits after the onset. The PW1 structure is obvious at the region from the North Pole to ~20°N before the onset, and the PW2 structure covers the whole northern hemisphere after the onset. The location of Langfang is within the range of the effects of the PW during 2013 SSW, which indicates that the anomalies of Langfang zonal winds from 20–100 km from MF radar and MERRA are indeed related with the 2013 SSW [29].

Figure 8 depicts longitudinal distributions of zonal wind along 40ºN for 4, 9 and 31 January 2013 in the top, middle and bottom panels of Figure 8 in the WACCM-SD simula-

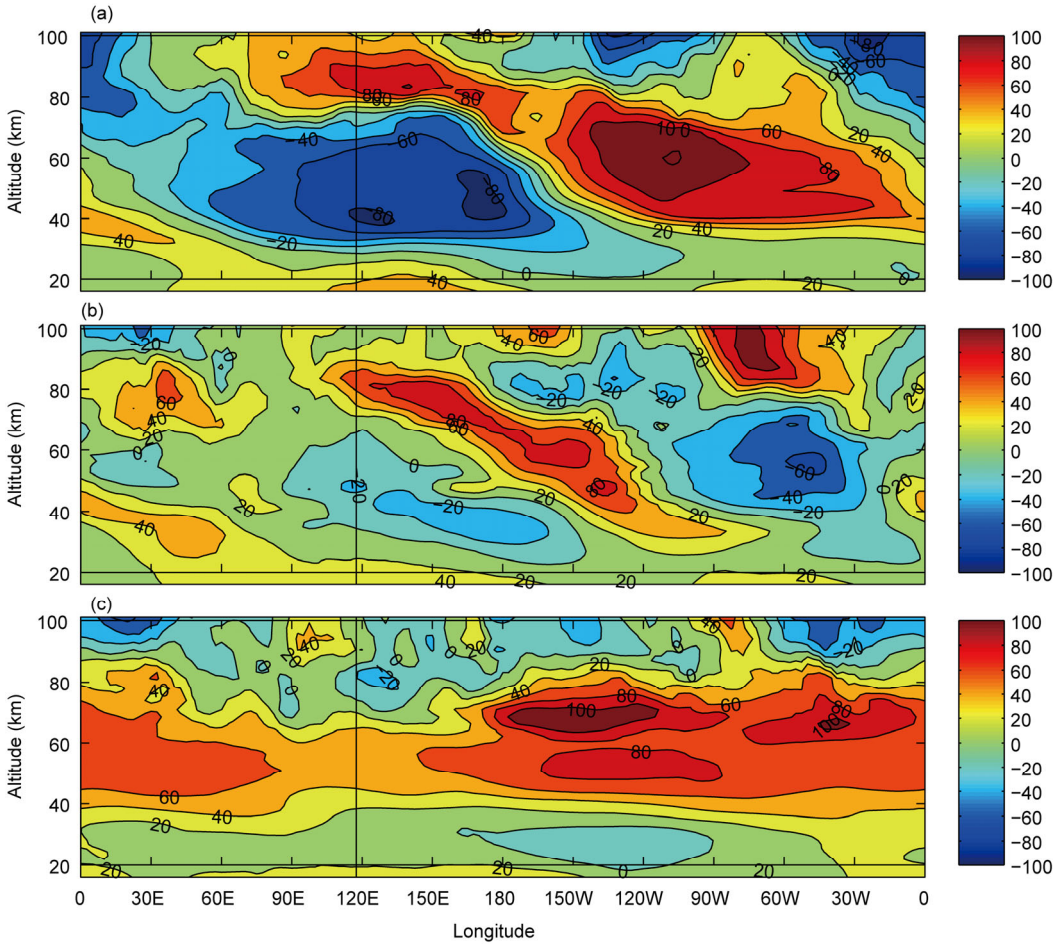

Figure 8 Longitudinal distributions of zonal wind (m/s) in the SD-WACCM simulation along 40ºN for 4 (a), 9 (b) and 31 (c) January 2013. The atmosphere at Langfang (39.4°N, 116.7°E) is indicated by thick and thin black straight line.

tion. Although the zonal wind zonal wind in the region 30–80 km decelerates or reverses during the SSW, there are large fluctuations of wind ranging between –100 to 100 m/s along the latitude circle. The zonal winds at mid-latitude 40°N show obviously PW1 and PW2 structures in Figure 8(a) and (b). With Figure 5, it can be confirmed the PW1 and PW2 of zonal winds surround the latitude circle before and after the onset respectively. In 4 January 2013 (Figure 8(a)), there is a peak westward wind appeared at near 120°E and a peak eastward winds occurred at near 120°W below 70 km, causing the reversal of winds over Langfang (indicated by a thick black straight line) which is not seen in most western hemisphere. After the onset (Figure 8(b)), two centers of strong westward wind and two centers of strong eastward wind are located at 150°E, 50°W and 40°E, 150°W in the stratosphere. In addition, the westward tilt of the PW1 and PW2 can be observed obviously during the SSW. As a consequence, the direction of zonal wind in MLT is always different with the wind below the region, which explains the acceleration (reversal) of zonal winds above (below) 60–70 km before the onset over Langfang and altitudinal anomalies of zonal wind after the onset. In 31 January (Figure 8(c)), the most regions 30–80 km at mid-latitude are dominated by the eastward wind after SSW.

In summary, while the zonal mean zonal wind decelerates as the result of westward forcing of planetary waves, there are differences in the local zonal wind along with the longitude depending on the position on the planetary waves. In 2013 SSW, when the PW1 dominates the atmosphere before the onset, the zonal wind reverses in one hemisphere, but not in the other hemisphere; when the PW2 dominates the atmosphere after the onset, the zonal wind reverses in some areas, but remains eastward in other areas. Furthermore, the tilt of planetary waves makes the altitudinal response of zonal wind to SSW more complicated.

Although we only give 2013 SSW simulation using the SD-WACCM in this paper, but the various responses described in Section 3.1 can be shown in Figure 8. Ignoring the yearly variability, the anomalies of zonal wind at Fort Collins during the 2009 SSW look like the structure at ~150°W in Figure 8(a) and (b). Since the 2010 SSW is dominated by PW1 [40], the wind response before (after) the onset at Langfang is similar as the structure at ~90°E

(~30°E) in the Figure 8(a).

Thus, we can safely come to the conclusion that the modulation of PW1 or PW2 plays the main role on the different zonal wind related to the SSWs. Different phases of PWs would lead to the different zonal wind at different longitudes and the different amplitudes and phases in different year would lead to the different zonal wind during different SSW events.

4 Conclusions

The evolution of zonal wind in the stratosphere, mesosphere and lower thermosphere at Langfang during the 2010 and 2013 SSW is investigated by a combination of continuous wind observations from MF radar and the wind data of MERRA over the same location. Comparisons are also made with zonal wind changes of Fort Collins during 2009 SSW, which shows various responses of zonal wind to SSWs in the stratosphere, mesosphere and lower thermosphere at ~40°N. The SD-WACCM is also applied for simulation of 2013 SSW to find the dynamics mechanism causing these changes during the SSWs.

The zonal mean zonal wind changes in the MERRA below 78 km over mid-latitude during different SSW events are similar that the wind decelerates or reverses. However, the responses at local observed sites are various before and after the onset of SSWs: the wind below 60–70 km at Langfang reverses from eastward to westward and accelerates above 60–70 km before the onset in 2010 and 2013 SSW, whereas the reversal region is only at 20–30 km at Fort Collins in 2009 SSW; after the onset, the stratosphere, mesosphere and lower thermosphere is covered by westward wind at Langfang in 2010 SSW, and eastward wind appears at 60–80 km over Langfang in 2013 SSW, and at 30–60 and 95–100 km for Fort Collins in 2009 SSW.

The SD-WACCM simulation captures the similar zonal wind feature as the combination of MF observation and MERRA during the 2013 SSW and is helpful to see how the PW induce the different anomalies. The simulation shows that the vortex exists at all altitude and covers the most northern hemisphere, indicating the anomalies at mid-latitude or Langfang are associated with the SSW. During the 2013 SSW, planetary waves of number 1 and 2 enhance dramatically extending to the middle latitude from 20 to 100 km before and after the onset respectively. The planetary waves produce westward forcing from the wave-flow interaction leading the deceleration or reversal of zonal mean zonal wind below 85 km.

Around the onset, when the zonal mean zonal wind decelerates to the weakest, there are still planetary wave of number 1 (such as 2010 SSW) or number 2 (such as 2013 SSW) at mid-latitude. The various responses at the observed sites during SSWs are decided by the position in the phases of PW1 or PW2. When the weak zonal mean winds are overlaid by the planetary waves, leading obvious eastward/westward directed winds in the longitudinal distributions at mid-latitude. The altitudinal responses at observed sites are also caused by the tilt of planetary waves.

Overall, the various responses to SSWs in the stratosphere, mesosphere and lower thermosphere at ~40°N are presented and one of the dynamics related with the anomalies is investigated in our study. Besides above work, the SSWs may cause the change of tides of 24 or 12 h [26]. The wind anomalies during the SSW are also influenced by the gravity waves, especially in the MLT [14]. Our future studies could be focused on these topics during SSW events with the co-located meteor radar, MF and sodium lidar at Langfang station. The simulations by WACCM are also useful to make a better understanding of the atmospheric response to the SSW from global view.

This work was supported by the National Natural Science Foundation of China (Grant No. 41104099). MERRA data used in this study have been provided by the Global Modeling and Assimilation Office (GMAO) at NASA Goddard Space Flight Center through the NASA GES DISC online archive. The GEOS-5 data used have been provided by the GMAO at NASA Goddard Space Flight Center through the online data portal in the NASA Center for Climate Simulation. We are grateful to the NCAR for the WACCM.

1 Scherhag R. Die explosionsartige Stratosphärenerwärmungen des Spätwinters 1951/52. Ber deut Wetterdienstes, 1952, 6: 51–63
2 Gerber E P, Butler A, Calvo N, et al. Assessing and understanding the impact of stratospheric dynamics and variability on the earth system. Bull Am Meteorol Soc, 2012, 93: 845–859
3 Hoffmann P, Singer W, Keuer D, et al. Latitudinal and longitudinal variability of mesospheric winds and temperatures during stratospheric warming events. J Atmos Sol Terr Phys, 2007, 69: 2355–2366
4 Smith A K, López-Puertas M, García-Comas M, et al. SABER observations of mesospheric ozone during NH late winter 2002–2009. Geophys Res lett, 2009, 36: L23804
5 Goncharenko L P, Chau J L, Liu H L, et al. Unexpected connections between the stratosphere and ionosphere. Geophys Res lett, 2010, 37: L10101
6 Xiao C Y, Hu X. Variability of the atmosphere during the sudden stratospheric warming observed by the COSMIC occultations. Chin J Space Sci, 2011, 31: 34–43
7 Smith A K. Global dynamics of the MLT. Surv Geophys, 2012, 33: 1177–1230
8 Gong Y, Zhou Q H, Zhang S D. Atmospheric tides in the low-latitude E and F regions and their responses to a sudden stratospheric warming event in January 2010. J Geophys Res Space Phys, 2013, 118: 7913–7927
9 Fagundes P R, Goncharenko L P, Abreu A J, et al. Ionospheric response to the 2009 sudden stratospheric warming over the equatorial, low, and middle latitudes in the South American sector. J Geophys Res, 2015, 120: 7889–7902
10 Wit R J, Hibbins R E, Espy P J, et al. Coupling in the middle atmosphere related to the 2013 major sudden stratospheric warming. Ann Geophys, 2015, 33: 309–319
11 Matsuno T. A dynamical model of the stratospheric sudden warming. J Atmos Sci, 1971, 28: 1479–1494
12 Yamashita C, Liu H L, Chu X Z. Responses of mesosphere and lower thermosphere temperatures to gravity wave forcing during stratospheric sudden warming. Geophys Res lett, 2010, 37: L09803
13 Limpasuvan V, Alexander M J, Orsolini Y J, et al. Mesoscale simula-

tions of gravity waves during the 2008–2009 major stratospheric sudden warming. J Geophys Res, 2011, 116: D17104
14 Wit R J, Hibbins R E, Espy P J, et al. Observations of gravity wave forcing of the mesopause region during the January 2013 major sudden stratospheric warming. Geophys Res lett, 2014, 41: 4745–4752
15 Yue J, Zhang S D, Yi F, et al. Observations of gravity wave activity during stratospheric sudden warming in the northern hemisphere. Sci China Tech Sci, 2015, 58: 951–960
16 Labitzke K. The interaction between stratosphere and mesosphere in winter. J Atmos Sci, 1972, 29: 1395–1399
17 Labitzke K. Stratospheric-mesospheric midwinter disturbances: A summary of observed characteristics. J Geophys Res, 1981, 86: 9665–9678
18 Bhattacharya Y, Shepherd G G, Brown S. Variability of atmospheric winds and waves in the arctic polar mesosphere in the arctic polar mesosphere during a stratospheric sudden warming. Geophys Res lett, 2004, 31: L23101
19 Siskind D E, Coy L, Espy P. Observations of stratospheric warmings and mesospheric coolings by the timed Saber instrument. Geophys Res let, 2005, 32: L09804
20 Limpasuvan V, Richter J H, Orsolini Y J, et al. The roles of planetary and gravity waves during a major stratospheric sudden warming as characterized in WACCM. J Atmos Sol Terr Phys, 2012, 78: 84–98
21 Kodera K. Influence of stratospheric sudden warming on the equatorial troposphere. Geophys Res Lett, 2006, 33: L06804
22 Shepherd M G, Wu D L, Fedulina I N, et al. Stratospheric warming effects on the tropical mesospheric temperature field. J Atmos Sol Terr Phys, 2007, 69: 2309–2337
23 Sathishkumar S, Sridharan S. Planetary and gravity waves in the mesosphere and lower thermosphere region over Tirunelveli (8.7°N, 77.8°E) during stratospheric warming events. Geophys Res Lett, 2009, 36: L07806
24 Yue J, Zhang S D, Yi F, et al. Variations of Kelvin waves around the TTL region during the stratospheric sudden warming events in the northern hemisphere winter. Ann Geophys, 2016, 34: 331–345
25 Jacobi C, Kürschner D, Muller H G, et al. Response of the mesopause region dynamics to the February 2001 stratospheric warming. J Atmos Sol Terr Phys, 2003, 65: 843–855
26 Chen X X, Hu X, Xiao C Y. Variability of MLT winds and waves over mid-latitude during the 2000/2001 and 2009/2010 winter stratospheric sudden warming. Ann Geophys, 2012, 30: 991–1001
27 Yuan T, Thurairajah B, She C Y, et al. Wind and temperature response of midlatitude mesopause region to the 2009 sudden stratospheric warming. J Geophys Res, 2012, 117: D09114
28 Hocke K, Lainer M, Schanz A. Composite analysis of a major sudden stratospheric warming. Ann Geophys, 2015, 33: 783–788
29 Chandran A, Collins R L. Stratospheric sudden warming effects on winds and temperature in the middle atmosphere at middle and low latitudes: A study using WACCM. Ann Geophys, 2014, 32: 859–874
30 Xiao C Y, Hu X, Xu Q C. Response of mesosphere and lower thermosphere wind over mid-latitude to the 2013 major sudden stratospheric warming event. In Proceedings of General Assembly and Scientific Symposium (URSI GASS), 2014 Beijing: IEEE, 2014
31 Xiao C Y, Hu X, Smith A K, et al. Short-term variability and summer-2009 averages of the mean wind and tides in the mesosphere and lower thermosphere over Langfang, China (39.4°N, 116.7°E). J Atmos Sol Terr Phys, 2013, 92: 65–77
32 Rienecker M M, Suarez M J, Gelaro R, et al. MERRA: NASA's modern-era retrospective analysis for research and applications. J Clim, 2011, 24: 3624–3648
33 Lindzen R S. Turbulence and stress owing to gravity wave and tidal breakdown. J Geophys Res, 1981, 86: 9707–9714
34 Beres J H, Garcia R R, Boville B A, et al. Implementation of a gravity wave source spectrum parameterization dependent on the properties of convection in the whole atmosphere community climate model (WACCM). J Geophys Res, 2005, 110: D10108
35 Garcia R R, Marsh D R, Kinnison D E, et al. Simulation of secular trends in the middle atmosphere, 1950–2003. J Geophys Res, 2007, 112: D09301
36 Richter J H, Sassi F, Garcia R R. Towards a physically based gravity wave source parameterization. J Atmos Sci, 2010, 67: 136–156
37 Marsh D. Chemical-dynamical coupling in the mesosphere and lower thermosphere. In: Aeronomy of the Earth's Atmosphere and Ionosphere. Netherlands: Springer, 2011. 3–17
38 Suarez M J, Rienecker M M, Todling R, et al. The GEOS-5 data assimilation system-documentation of versions 5.0.1, 5.1.0. Technical Report. Greenbelt: NASA Goddard Space Flight Center, 2008. NASA/TM-2008-104606-VOL-27
39 Andrews D G, Holton J R, Leovy C B. Middle Atmospheric Dynamics. San Diego: Academic, 1987. 123–133
40 Ayarzagüena B, Langematz U, Serrano E. Tropospheric forcing of the stratosphere: A comparative study of the two different major stratospheric warmings in 2009 and 2010. J Geophys Res, 2011, 116: D18114